Eur. Phys. J. B **34**, 293–303 (2003)
DOI: 10.1140/epjb/e2003-00225-1

THE EUROPEAN PHYSICAL JOURNAL B

Slow-fast dynamics in Josephson junctions

E. Neumann[a] and A. Pikovsky

Department of Physics, University of Potsdam, Am Neuen Palais, PF 601553, 14415, Potsdam, Germany

Received 10 March 2003
Published online 11 August 2003 –

Abstract. We report on a nontrivial type of slow-fast dynamics in a Josephson junction model externally shunted by a resistor and an inductor. For large values of the shunt inductance the slow manifold is highly folded, and different types of dynamical behavior in the fast variable are possible in dependence on the other parameters of the junction. We discuss how particular features of the dynamics are manifested in the current-voltage characteristics of the shunted junction.

PACS. 05.45.-a Nonlinear dynamics and nonlinear dynamical systems – 85.25.Cp Josephson devices – 74.81.-g Inhomogeneous superconductors and superconducting systems

1 Introduction

Resistively shunted Josephson junctions appear in many applications, as for instance in Josephson junction arrays and ladders [1–3] and in superconducting quantum interference devices (SQUIDs) [4]. The simplest possible model to describe the dynamics of a Josephson junction is the resistively and capacitively shunted junction (RCSJ) model where a resistor and a capacitor are shunted parallely to the ideal Josephson junction flown through by the supercurrent. However, if the resistive shunt due to its wiring contains a non-negligible inductance, the well-known RCSJ model fails to describe the current-voltage characteristics of the junction. Such an inductance has to be accounted, *e.g.* in the case of the SQUID [4] where a single Josephson junction is closed with a superconducting loop.

Moreover, it has been shown that measurements of the current-voltage characteristics of a Josephson junction not being closed by a superconducting loop are well represented by numerical simulations of the RCSJ model only below a certain temperature [5]. For higher temperatures, anomalies in the characteristics have been found, that can be ascribed to the finite inductance in the shunt. Consequently, in order to remedy this lack, a resistive-capacitive-inductive junction (RCLSJ) model has been suggested to describe these junctions [5,6]. Consideration of this model leads to a better agreement of the numerical simulations with the experimentally obtained data. Only for large values of the shunt resistance one can expect almost RCSJ-like current-voltage curves no matter which value of the inductance is present.

The dependence of the dynamics on the strength of the inductance has been considered [6,7]. It has been found that chaotic solutions can be expected at low values of the inductance, whereas for intermediate values long chaotic transients precede periodic oscillations. For high inductance values the dynamics has been found to be dominated by relaxation oscillations [5]. Such type of oscillations can also be observed in the resistive single junction interferometer (SQUID) [4].

Numerical simulations of the RCLSJ model have been used to reproduce the qualitative features of the current-voltage characteristics [7,8]. Based on this, a method has been suggested to determine the device parameters such as the capacitance and the inductance of the junction. Indeed, measurements of the instantaneous voltage across the junction are impossible since the characteristic time scale is in the order of picoseconds. Only the measurements of the dc voltage in dependence on the varied net current are possible and can be compared with numerically obtained current-voltage characteristics. In this way one can show that anomalies in the current-voltage curves are caused by particular relaxation oscillations and complex voltage waveforms [8]. Furthermore, the inductively shunted junction model forced by an external ac signal has been considered in [9].

In this article we investigate the dynamics of the RCLSJ model in the presence of small parameters which allow us to separate slow and fast motions. In particular, the shunt resistance is assumed to be small. Then, the type of the dynamics is described in dependence on the parameters characterizing the capacitance and the shunt inductance, respectively. We will demonstrate that depending on these parameters one can observe different types of slow-fast dynamics. Coexistence of slow and fast motions is well known from self-sustained oscillators like the van der Pol oscillator and excitable systems like the Fitz Hugh-Nagumo model. Moreover, models

[a] e-mail: eireen@stat.physik.uni-potsdam.de

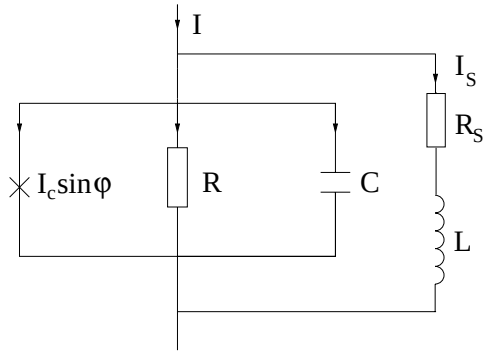

Fig. 1. The schematic representation of the RCLSJ model. The Josephson junction is represented by the supercurrent channel $I_c \sin\varphi$, the normal resistance R, and the junction capacitance C. The inductive shunt consists of a resistor R_S in series with an inductance L.

describing activator-inhibitor systems in biological issues like the spiking-bursting neuronal activity [10,11] show slow-fast dynamics. In these models, at certain parameter values a limit cycle can be observed consisting of two pieces of slow motion connected with fast jumps. We will demonstrate that the motions in the RCLSJ model are more complex because the fast manifold can be two-dimensional.

We do not consider the most general formulation of the problem, instead concentrating on the aspects of the dynamics. In particular we assume that the magnetic field is absent, and that the resistance is linear; see [5–9] for more general formulation.

The paper is organized as follows: In the following Section 2 we introduce the model and derive the equation of motion. The choice of parameters is discussed with respect to the possibility to observe slow-fast dynamics. Then, in Section 3 the dynamics is analysed for three types of damping. The current-voltage characteristics is discussed, and is analysed in its relation to the dynamics. Finally, the results are summarized in Section 4.

2 Model

2.1 Basic equations

The system under consideration, the RCLSJ model of a Josephson junction, is sketched in Figure 1. The inner circuit represents the simple RCSJ model; here the ideal Josephson junction is flown through by the supercurrent $I_C \sin(\varphi)$ without any resistance. Since in real applications a voltage appears across the junction which can be time dependent, the ideal junction is shunted parallely by a resistor R and a capacitor C. Although dynamics of real junctions can be reproduced in many cases by this simple model, some additional special features of experimentally observed current-voltage curves appear if the shunt of the junction contains a non-negligible inductive component. To make the electronic circuit model more realistic, the outer shunt is accounted containing the shunt resistance R_S in series with the shunt inductance L. So this model, in fact, represents an upgrade of the usual RCSJ model.

The dynamics is described by the following equations [8]:

$$I = C\frac{dV}{dt} + \frac{V}{R} + I_c \sin\varphi + I_S,$$
$$V = \frac{\hbar}{2e}\frac{d\varphi}{dt} = L\frac{dI_S}{dt} + I_S R_S. \tag{1}$$

Here, I is the net current flowing through the junction and φ is the phase difference between the complex wave functions of the Cooper pairs in two pieces of superconductor constituting the junction, called Josephson phase. The shunt current I_S passes the shunt resistance R_S and the shunt inductance L that models the wiring of the resistor. The voltage V across the junction is determined by the second equation of equation (1) and is related to the time derivative of the Josephson phase $\dot{\varphi}$ by the well-known phase-voltage relation. Thus, the expressions containing voltage V can be rewritten in terms of the Josephson phase φ. Then, for reasons of convenience of analytical and numerical investigation let us transform equation (1) to a dimensionless form:

$$\beta\gamma^2\frac{d^2\varphi}{d\tau^2} + \gamma\frac{d\varphi}{d\tau} + \sin\varphi = J - i_S,$$
$$\frac{d\varphi}{d\tau} = \alpha\frac{di_S}{d\tau} + i_S. \tag{2}$$

Here we normalized time $\tau = \omega_S t$ with $\omega_S = 2eI_C R_S/\hbar$ as well as currents I_S and I with respect to the maximum amplitude of the supercurrent I_c: $J = I/I_c$, $i_S = I_S/I_c$. Actually, the normalized net current J can be time-dependent but we concentrate in the following on a simpler case and restrict ourselves on a constant value of J from now on. In equation (2) three parameters α, β, and γ have been introduced, they are defined as follows.

Parameter

$$\alpha = \frac{2eI_cL}{\hbar} \tag{3}$$

represents a dimensionless inductance, because $\frac{\hbar}{2eI_c}$ can be regarded as an intrinsic inductance L_0 of the Josephson junction. Parameter

$$\beta = \frac{2eI_cR^2C}{\hbar} \tag{4}$$

is the Stewart-McCumber parameter of the circuit without the outer shunt. It is in fact a reduced capacitance and measures the damping of the system ($\beta \to 0$ corresponds to high damping). The third parameter γ designates the ratio of the shunt resistance to the intrinsic one

$$\gamma = R_S/R. \tag{5}$$

As mentioned in the introduction (Sect. 1), system (2) has already been considered in references [5–9]. However, there

the damping parameter has been defined in a different way:

$$\beta_S = \frac{2eI_C R_S^2 C}{\hbar}, \tag{6}$$

containing the shunt resistance R_S. In terms of $\beta_S = \beta\gamma^2$, the system modeling the dynamics of the Josephson junction reads

$$\begin{aligned} \beta_S\ddot{\varphi} + \gamma\dot{\varphi} + \sin\varphi &= J - i_S, \\ \dot{\varphi} &= \alpha\frac{di_S}{d\tau} + i_S. \end{aligned} \tag{7}$$

A disadvantage of equation (7) is that the shunt resistance R_S is now contained in two different dimensionless parameters, namely in β_S and γ. Thus, from experimental point of view, a change of the shunt resistance R_S leads to some shift in the parameter plane (β_S, γ), *i.e.* to a change of both parameters β_S and γ. According to our definition (4), a change of R_S results in the variation of only one parameter γ, if we assume the intrinsic resistance R to be a constant. For a possible experimental check of the results concerning the dynamics and current-voltage characteristics, the dimensionless parameters α, β, and γ can be transformed easily to corresponding values of the shunt inductance L, the capacitance C, and shunt resistance R_S of the experimental setup and *vice versa.*

It is appropriate to write the system in terms of β (Eq. (2)) not only from the experimental point of view, but also with respect to the analysis of slow-fast dynamics of the system. For our way of defining the dimensionless parameters, it is obvious that γ should serve as the small parameter of the system. In contrast, system (7) is unsuitable for investigating slow-fast dynamics because it is not clear how to chose a small parameter.

Before analyzing system (2) with a restriction of parameter γ being small, let us consider a limiting case where the inductance L of the shunt is negligibly small. Then, the dynamical equations should reduce to these of the RCSJ model. According to equation (3), a negligibly small inductance L corresponds to the limit $\alpha \to 0$. From the second equation of equation (2) we obtain in this case $\dot{\varphi} = i_S$, thus the dynamics is described by a single differential equation of second order,

$$\beta\gamma^2\ddot{\varphi} + (\gamma+1)\dot{\varphi} + \sin\varphi = J. \tag{8}$$

After backscaling time by $t = \tau/\omega_S$, we obtain the differential equation

$$\frac{\hbar C}{2eI_c}\ddot{\varphi} + \frac{\hbar}{2eI_c}\left(\frac{1}{R_S} + \frac{1}{R}\right)\dot{\varphi} + \sin\varphi = J, \tag{9}$$

corresponding to the RCSJ model not accounting for the external inductivity of the junction. It describes the dynamics of an ideal Josephson junction shunted by a capacitor C and two resistors, R_S and R.

2.2 Transformation of the basic equations

The analysis of equation (2) is not obvious because it is not a system of ordinary differential equations (ODEs) in a standard form. There are many ways to write it as a system of ODEs but the most appropriate one for the analysis below is to introduce a supplementary variable $u = J - i_S + \frac{1+\gamma}{\alpha}\varphi + \frac{\beta\gamma^2}{\alpha}\dot{\varphi}$. This kind of transformation ensures that slow and fast manifolds are perpendicular to each other as is demonstrated below. Moreover, parameters β and γ occur only in the first equation of the two ODEs:

$$\begin{aligned} \beta\gamma^2\ddot{\varphi} + \gamma\left(1 + \frac{\beta\gamma}{\alpha}\right)\dot{\varphi} + \frac{1+\gamma}{\alpha}\varphi + \sin\varphi &= u, \\ \dot{u} &= \frac{1}{\alpha}(J - \sin\varphi). \end{aligned} \tag{10}$$

Equation (10) can be transformed into a system of three ODEs of first order that can be integrated using standard algorithms. It describes the time evolution of the Josephson phase φ and its first derivative $\dot{\varphi}$ as well as the dynamics of the just introduced new variable u.

In addition to the external normalized net current J, the dynamics is characterized by the three parameters α, β, and γ. It is convenient to consider parameter γ as the small parameter being contained in the terms including first and second derivatives of variable φ in equation (10) in corresponding power. Thus, the characteristic time scale the variable φ evolves on, is of the order γ whereas variations in variable u are characterized by a time scale of the order α. Therefore, the Josephson phase φ can be identified as the fast variable and u as the slow one, provided $\gamma \ll \alpha$ The variable φ is the more rapid the smaller the value of γ is. In the limit $\gamma \to 0$ the fast motion in φ becomes instantaneous, and we arrive at the simplified model

$$\begin{aligned} u &= \frac{1}{\alpha}\varphi + \sin\varphi, \\ \dot{u} &= \frac{1}{\alpha}(J - \sin\varphi), \end{aligned} \tag{11}$$

characterizing only the slow motion. Equation (11) consists of an algebraic equation describing the shape of the slow manifold $u = u(\varphi)$ and a differential equation for the time evolution on this slow manifold.

The shape of the slow manifold u is determined by parameter α. For $\alpha < 1$ the function $u = u(\varphi)$ is bijective, *i.e.* φ is a function of u, too. An example for this case is presented in Figure 2a. The situation changes at $\alpha = 1$, then φ is multivalued at values $u_k = \pi + 2k\pi$, these points are the inflection points of the function $u(\varphi)$. For $\alpha > 1$, the slow manifold $u(\varphi)$ becomes folded. This is an interesting and nontrivial case, where one can expect slow-fast dynamics to occur. A trajectory follows the slow manifold u up to its local maximum and then a fast jump of the variable φ along the fast manifold to another branch of the slow manifold is expected to occur .

For $\alpha > \alpha_1 \approx 4.61$, φ is multivalued at any value of u (Fig. 2b). As we will see below, this is important for certain phenomena to be observed in the slow-fast dynamics.

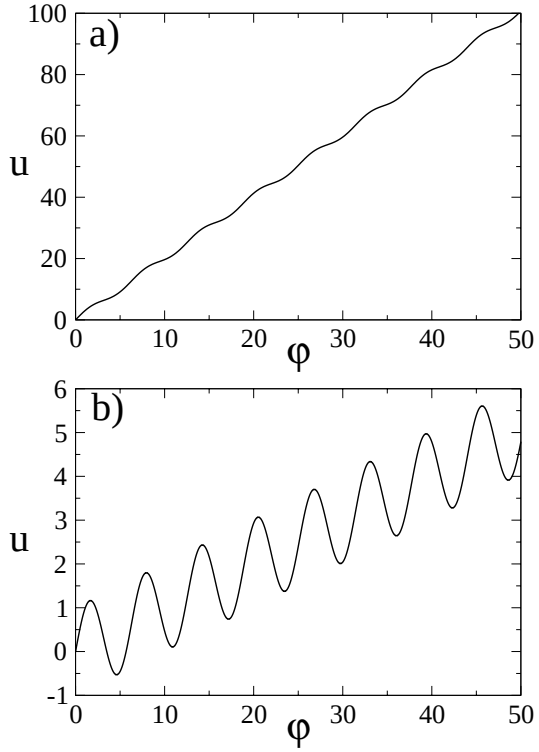

Fig. 2. Shape of the slow manifold $u = u(\varphi)$ in dependence on the value of the reduced inductance parameter α of the Josephson junction. For a) $\alpha = 0.5 < 1$ the function u is bijective, and for b) $\alpha = 10 > 1$ the function $u(\varphi)$ is folded.

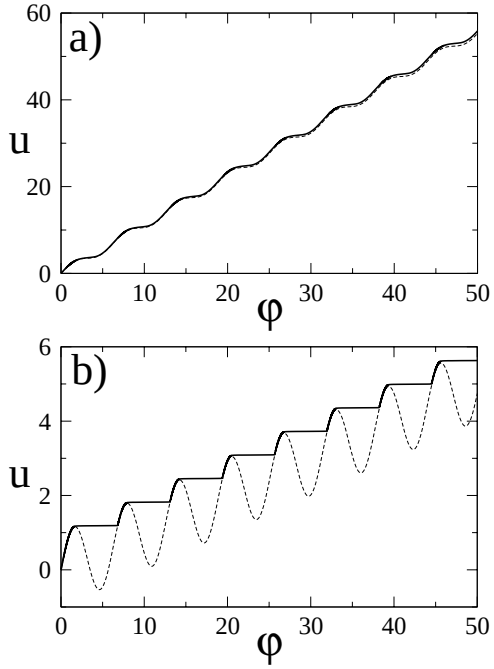

Fig. 3. Types of dynamics in the high damping limit. For a) $\alpha = 0.9 < 1$ the trajectory follows the slow manifold, whereas for b) $\alpha = 10 > 1$ slow-fast dynamics can be observed.

3 Dynamics and current-voltage characteristics

Before discussing the different features of slow-fast motion let us describe a range of parameters we are going to consider in this section. As already mentioned, parameter γ is assumed to be small, *i.e.* $\gamma \ll 1$. With regard to parameter α, we consider the interesting case $\alpha > \alpha_1 \approx 4.61$, where the motion on slow and fast time scales can be observed.

The Stewart-McCumber parameter β determines the strength of damping. We will discuss three types of damping in detail, namely the high damping limit ($\beta \ll 1$), intermediate damping ($\beta > 1$), and the low damping limit ($\beta \gg 1$). The current-voltage characteristics reflecting the dependence of the dynamics on the normalized net current J is analysed for these three types of damping, and the dynamical features are discussed.

3.1 High damping limit

In the high damping limit $\beta \to 0$, equation (10) reduces to a set of two first-order differential equations:

$$\begin{aligned} \gamma\dot{\varphi} &= u - \frac{1+\gamma}{\alpha}\varphi - \sin\varphi, \\ \dot{u} &= \frac{1}{\alpha}\left(J - \sin\varphi\right). \end{aligned} \tag{12}$$

Thus, the system of the overdamped Josephson junction (Eq. (12)) is of the same type as typical systems demonstrating slow-fast dynamics (*e.g.* the FitzHugh-Nagumo model) since it is characterized by the small parameter at the first derivative of one variable out of two.

Let us consider the solution of (12) for two values of α, $\alpha = 0.9$ and $\alpha = 10$, respectively. The structure of the slow manifold for these values of α differs as pointed out in the previous section. Therefore, the phase portraits (u, φ) presented in Figures 3a, b show different types of dynamics. In the case $\alpha < 1$ the trajectory follows the slow manifold (Fig. 3a), the motion on $u = u(\varphi)$ is uniform. For $\alpha > 1$ (Fig. 3b), due to the folded structure of the slow manifold, the slow-fast dynamics is observed. In this case the motion takes place on two different well separated time scales. Slow motion along stable branches of the slow manifold u alternates periodically with fast jumps in φ. Note that the fast motion is one-dimensional and tangential to the direction of slow motion at local maxima of function $u = u(\varphi)$. For large α, the jump length in the fast variable φ is approximately 2π whereas φ changes only slightly during motion on the slow manifold.

In order to estimate the current-voltage characteristics, the mean voltage $\langle\dot{\varphi}\rangle$ has to be computed in dependence on the net current J. Figure 4 shows the current-voltage curves for two different values of α, $\alpha = 2$ and $\alpha = 10$, respectively. No matter which value of α is accepted, for $J < 1$ the mean voltage across the junction is zero ($\langle\dot{\varphi}\rangle = 0$). Thus, a supercurrent flows through the junction without any resistance. Dynamically it means that the Josephson phase φ approaches a fixed point. The

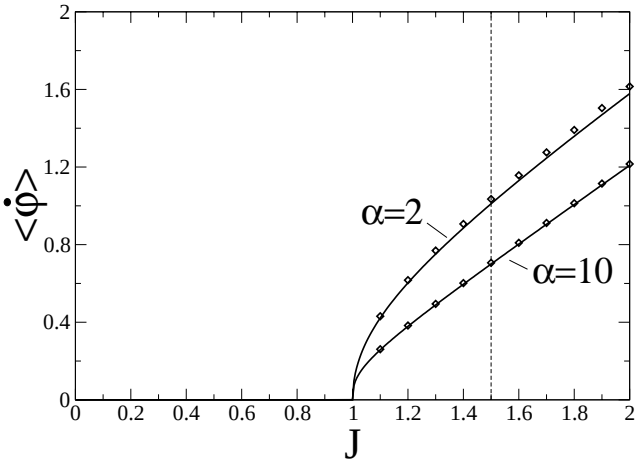

Fig. 4. The current-voltage characteristics in the high damping limit for $\alpha = 2$ and $\alpha = 10$. For $J < 1$ the mean voltage across the junction is zero, for $J > 1$ the junction is in the resistive state, where the resistance depends on α. The dashed vertical line marks the value $J = 1.5$ for which the time dependence of φ is presented in Figures 5a, b. For several values of J, the semi-analytically estimated values of the mean voltage are marked by diamonds for $\alpha = 2$ and $\alpha = 10$.

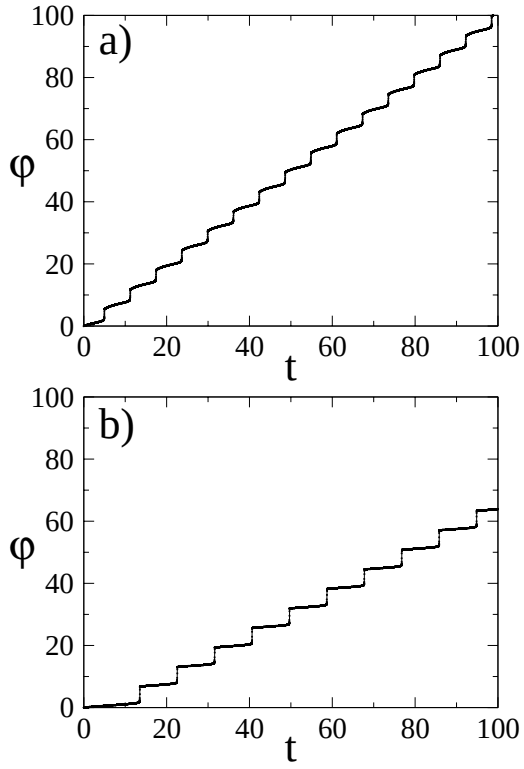

Fig. 5. Time dependence of the Josephson phase φ at $\gamma = 0.01$, $J = 1.5$, and a) $\alpha = 2$, and b) $\alpha = 10$. The mean slope and thus the mean voltage across the junction depends on α.

fixed point coordinates $(\bar{\varphi}, \bar{u})$ are given by $\bar{\varphi} = \arcsin J$ and $\bar{u} = \frac{1+\gamma}{\alpha}\bar{\varphi} + J$. In contrast, for $J > 1$, the junction is in the resistive state, *i.e.* a nonzero mean voltage $\langle\dot{\varphi}\rangle$ appears across the junction. Thus, the characteristics consists of two branches, the supercurrent branch and the resistive one. For two values of α, $\alpha = 2$ and $\alpha = 10$, the time dependence of the Josephson phase φ is presented in Figures 5a, b at the same value of the net current $J = 1.5$. Both dependences reflect the periodic repetition of the fast jumps in φ by approximately 2π, but the mean slope and, thus, the mean voltage across the junction differ. At the same value of J one observes that for large α, the mean voltage $\langle\dot{\varphi}\rangle$ is small. The mean voltage can be computed as well semi-analytically as is shown below. First, our goal is to estimate the duration of the slow motion. To this end, we assume that the fast jumps are instantaneous, *i.e.* $\gamma = 0$. Then, equation (12) reduces to equation (11), and the expression for the slow manifold (first equation of (11)) is differentiated with respect to time, and $\dot{u}$ is substituted to obtain

$$\dot{\varphi} = \frac{J - \sin\varphi}{1 + \alpha\cos\varphi}. \tag{13}$$

Integration of this equation yields

$$\begin{aligned} T &= \int_{\varphi_1}^{\varphi_2} \frac{(1+\alpha\cos\varphi)d\varphi}{J-\sin\varphi} \\ &= -\frac{2\mathrm{atan}\left(\dfrac{\sec(\varphi/2)(\cos(\varphi/2) - J\sin(\varphi/2))}{\sqrt{J^2-1}}\right)}{\sqrt{J^2-1}}\Bigg|_{\varphi_1}^{\varphi_2} \\ &\quad - \alpha\ln(J-\sin\varphi)|_{\varphi_1}^{\varphi_2}. \end{aligned} \tag{14}$$

To estimate the period T we have to find the limits of integration φ_1 and φ_2 being the limits of the phase interval within which the slow motion takes place. For explanation of the estimation of this interval see Figures 6a, b where the trajectory in the phase space (φ, u) is sketched for $\alpha = 2$ and $\alpha = 10$, respectively.

The periods of slow motion end at those values of φ for which the function $u(\varphi) = \varphi/\alpha + \sin(\varphi)$ has local maxima. Just at these values $\varphi_{2n} = 2\pi n + \arccos(-1/\alpha)$ the fast jumps in φ start. In Figures 6a, b the first two fast jumps are presented, starting at $\varphi_c = \varphi_0 = \arccos(-1/\alpha)$ and $\varphi_2 = 2\pi + \arccos(-1/\alpha)$, respectively. The first fast jump starting from $(\varphi_c, u_c = u(\varphi_c))$ ends at (φ_1, u_c) on the next branch of the slow manifold. Thus, the subsequent period of slow motion along $u(\varphi)$ is limited by (φ_1, u_c) and $(\varphi_2, u(\varphi_2))$. The still needed estimation of φ_1 leads to a transcendent equation, $u_c = \varphi/\alpha + \sin(\varphi)$ which cannot be solved analytically. However, we can find its root numerically.

Now, having the values φ_1 and φ_2 for $\alpha = 2$ and $\alpha = 10$, the duration T of slow motion can be computed according (14) for each α. This has been done for several values of the net current $J \in (1, 2]$ for both values of α.

Then, the mean voltage can be estimated by

$$\langle\dot{\varphi}\rangle = \frac{2\pi}{T} \tag{15}$$

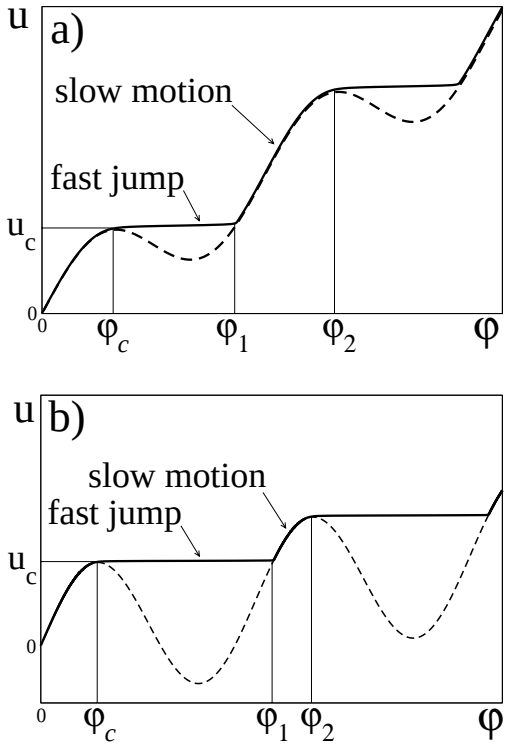

Fig. 6. Visualization of slow and fast motion in the phase space (φ, u). For a) $\alpha = 2$ the phase interval (φ_1, φ_2) of slow motion is larger than for b) $\alpha = 10$. The fast jump in the Josephson phase φ can be approximated by 2π the better the larger α is.

because the period in φ is equal to 2π. Using the data of period T computed for both values of α, the corresponding values of the voltage $\langle\dot{\varphi}\rangle$ have been estimated according to expression (15) and marked in Figure 4 by diamonds. The semi-analytically estimated values of the mean voltage confirm those obtained by integrating system (12). Note, that the deviation from the purely numerically obtained resistive branch of the characteristics becomes larger for increased J. The assumption that the fast jump happens instantaneously is more reliable the larger α is. Therefore, the deviation is smaller for $\alpha = 10$ than for $\alpha = 2$.

3.2 Intermediate damping

For intermediate damping ($\beta \gtrsim 1$) the dynamics of the Josephson junction is described by equation (10). Again, one can expect to observe slow-fast dynamics since parameter γ is assumed to be small. However, the jump in the fast variable φ depends now on the damping parameter β. We do not only observe jumps by approximately 2π (Fig. 7a), but also by multiples of 2π (Figs. 7b, c) at $\alpha = 10$.

Let us have a closer look onto the structure of the slow manifold (Fig. 8). It consists of stable and unstable branches. The trajectory follows the slow manifold along the stable branch up to its first local maximum, denoted by u_c. Then the first fast jump would occur in the direction marked by the arrow which crosses three stable branches. Depending on the value of β, the jump length can be approximately 2π, 4π or 6π corresponding to the first, second and third crossing of stable branches, respectively. It is obvious that for large values of α, the slow manifold is stronger folded and more crossings can occur. Hence, jumps by higher multiples of 2π can be expected to happen. On the other hand, for $\alpha < \alpha_1 \approx 4.61$, when the slow manifold is not folded strong enough and the arrow would not cross any stable branch, we could observe only jumps by 2π in φ as in the high damping limit. In that

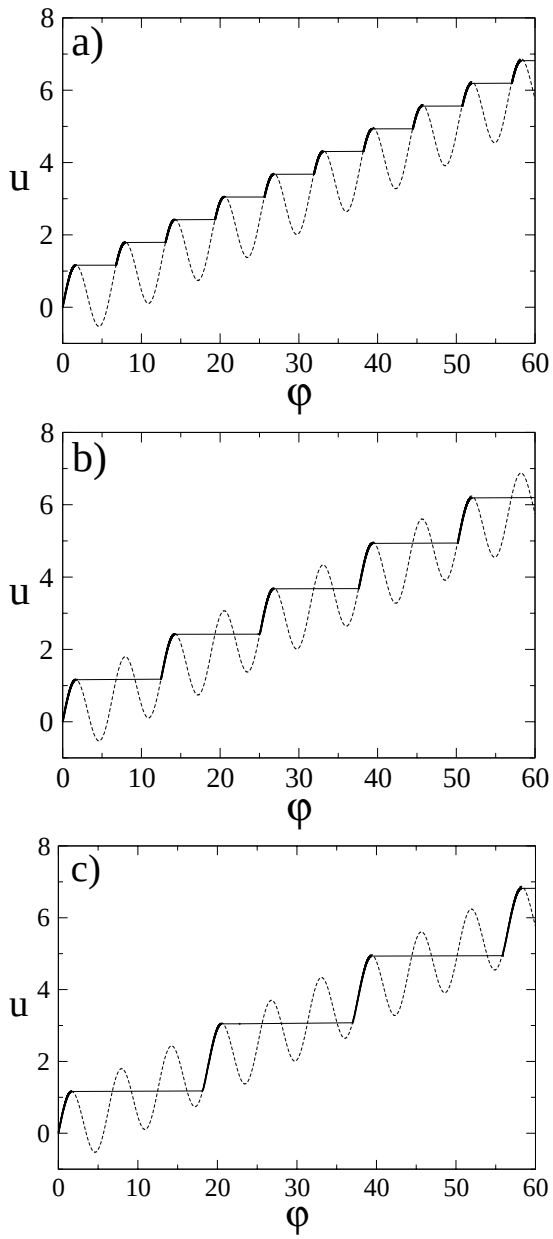

Fig. 7. Different jump length in the Josephson phase in dependence on the strength of damping. One observes at a) $\beta = 2$ jumps by $\approx 2\pi$, b) $\beta = 40$ jumps by $\approx 4\pi$ and c) $\beta = 130$ jumps by $\approx 6\pi$. The other parameters are $\alpha = 10$, $\gamma = 10^{-4}$ and $J = 1.5$.

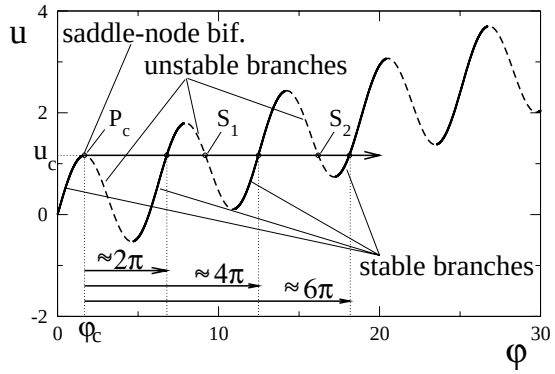

Fig. 8. Structure of the slow manifold. Stable branches are presented by solid lines, unstable branches by dashed lines. The arrow shows the direction of an instantaneous jump whose length depends on the value of damping parameter β.

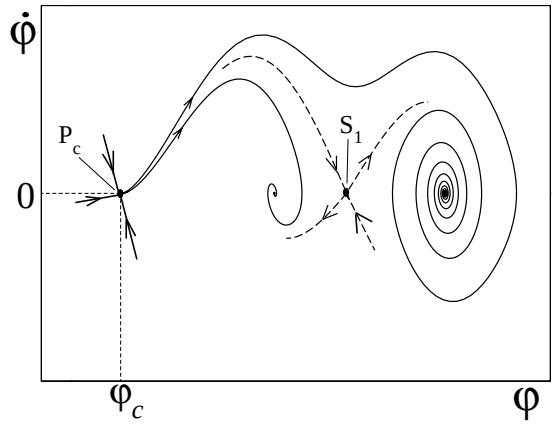

Fig. 9. Schematic representation of the unstable trajectory of the semi-stable point $P_c = (u_c, \varphi_c, \dot{\varphi} = 0)$ (solid line) for two different values of β. This trajectory can go to one or another stable fixed point depending on its position relative to the stable manifold of the saddle point S_1 (dashed line). As a result, fast motion can lead to a jump of φ by $\approx 2\pi$ or $\approx 4\pi$.

case, the jump dynamics would be qualitatively independent of the value of damping parameter β.

Provided that the slow manifold is folded strong enough to make slow-fast dynamics possible, what type of mechanism is responsible for the jump length? In order to answer this question we consider the fast motion of the first jump taking place in the subspace $(u = u_c, \varphi, \dot{\varphi})$ in more detail. A schematic representation of the topology around the point $P_c = (u_c, \varphi_c, \dot{\varphi} = 0)$ from where the first fast jump starts is presented in Figure 9. At P_c a saddle-node bifurcation occurs, *i.e.* stable and unstable fixed points collide there, and then both disappear (typically a stable point is a focus, but in the vicinity of bifurcation point it becomes a node).

In the intersection plane $(u_c, \varphi, \dot{\varphi})$, the point P_c is a semi-stable point, characterized by only one unstable trajectory. As observed, the different jump length depends on the value of β. In Figure 9 two different trajectories (at two different values of β) starting from P_c and seperatrices (dashed curves) of the saddle point S_1 are sketched. This saddle point S_1 is just the intersection point of the plane $(u_c, \varphi, \dot{\varphi})$ with the first unstable branch next to P_c (see Fig. 8). Obviously, the jump length depends on whether the unstable trajectory is above or below the stable manifold of saddle point S_1. For small β it is below, and the jump length is approximately 2π. For larger β, the trajectory moves above the stable manifold of S_1, thus the jump length changes and becomes larger than 2π. The same mechanism just described underlies the behavior of trajectories near the second saddle point S_2 even though it is omitted in Figure 9 for clarity of representation.

To prove these theoretical considerations, let us decouple the fast jump dynamics from the slow motion by observing the system (10) only on the fast time scale. The corresponding transformation to the time scale $t = \gamma\tau$ and subsequent consideration of the dynamics in the limit $\gamma \to 0$ cause that only variations of the fast variable φ are visible while the slow variable u is quasiconstant. Thus, the time evolution of the fast variable φ is given by

$$\beta\ddot{\varphi} + \dot{\varphi} + \frac{1}{\alpha}\varphi + \sin\varphi = u_c, \tag{16}$$

where u_c is just the value on the slow manifold from where the first fast jump occurs. The dynamics now starts at corresponding value φ_c with velocity $\dot{\varphi} = 0$ (it is the initial voltage across the junction). Hence, the first fast jump starting from P_c can be simulated numerically. The crossing points of the plane $(u_c, \varphi, \dot{\varphi})$ (presented by the arrow in Fig. 8) with stable and unstable branches of the slow manifold mark positions of foci and saddles in the $(\varphi, \dot{\varphi})$ phase plane. By forward and backward integration of equation (16) in time, for saddle locations S_1, S_2 as initial values of φ and initial zero voltage $\dot{\varphi} = 0$, the stable and unstable manifolds of the saddles S_1 and S_2 in the $(\varphi, \dot{\varphi})$ plane have been computed (see Fig. 10). Thus, we find different connections between the foci and saddles. Then, simulating the dynamics with the initial values $(\varphi_c, \dot{\varphi} = 0)$, the trajectory representing the jump dynamics has been generated. So, one obtains the phase portraits of the fast motion in the $(\varphi, \dot{\varphi})$ phase plane in dependence on the damping parameter β (Figs. 10a–d). We observe that the fast dynamics is two-dimensional in contrast to that in the high damping limit. Moreover, due to the variation of β, the topology of the connections between foci and saddles changes; the stable and unstable manifolds wind around the saddles and foci and come nearer to each other as β is increased, *i.e.* for lowering the dissipation (compare Figs. 10a–d). This topology in fact causes the different jump lengths ($\Delta\varphi \approx 2\pi, 4\pi, 6\pi$).

For the just considered limiting case $\gamma = 0$, the jump dynamics is well defined. The regions of phase jumps of different length in the (β, J) parameter plane are estimated in dependence on β, and presented in Figure 11a. The borders between different regions do not depend on the net current J because the whole dynamics is independent of J (see Eq. (16)). They are parallel to the J-axes.

This situation changes if we do not restrict our observation onto the fast dynamics but account for the influence of the slowly varying variable u ($\gamma \neq 0$) on the fast

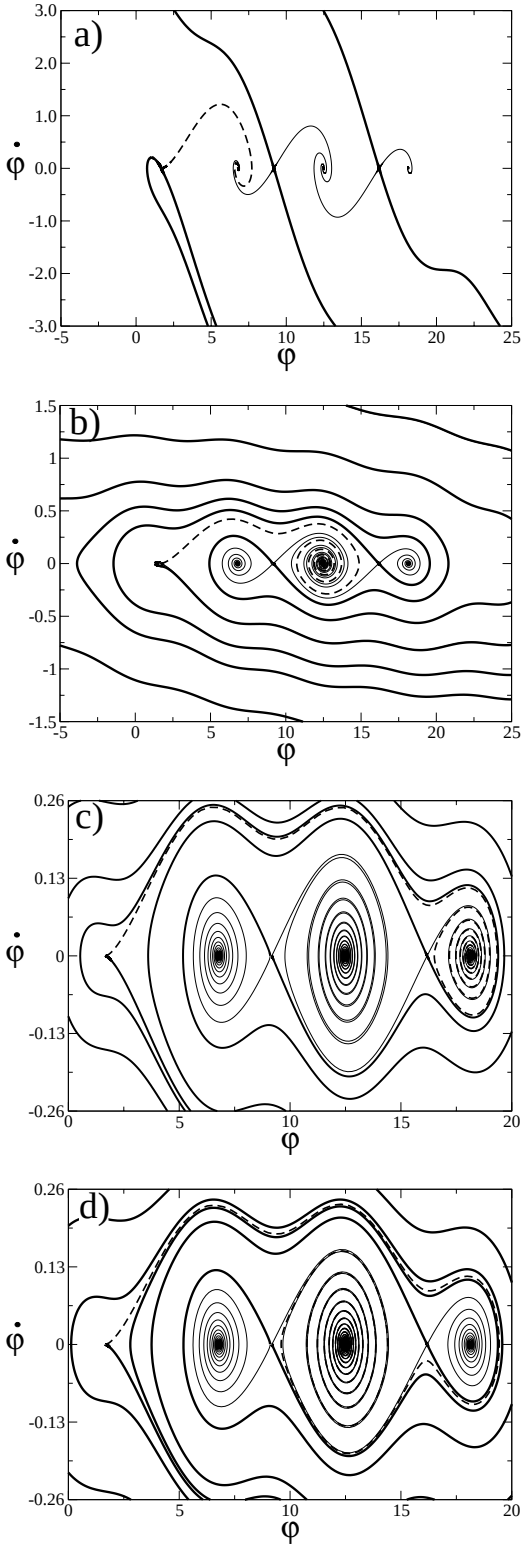

Fig. 10. The phase portraits in the $(\varphi, \dot{\varphi})$ phase plane in dependence on the damping parameter β, the observed jump length at a) $\beta = 2$ is $\Delta\varphi \approx 2\pi$, at b) $\beta = 40$ is $\Delta\varphi \approx 4\pi$, at c) $\beta = 130$ is $\Delta\varphi \approx 6\pi$ and at d) $\beta = 150$ is $\Delta\varphi \approx 4\pi$. The stable manifolds (thick lines) and unstable manifolds (thin lines) represent the different connections between the saddles and foci. The trajectory representing the jump dynamics is shown by dashed thick line.

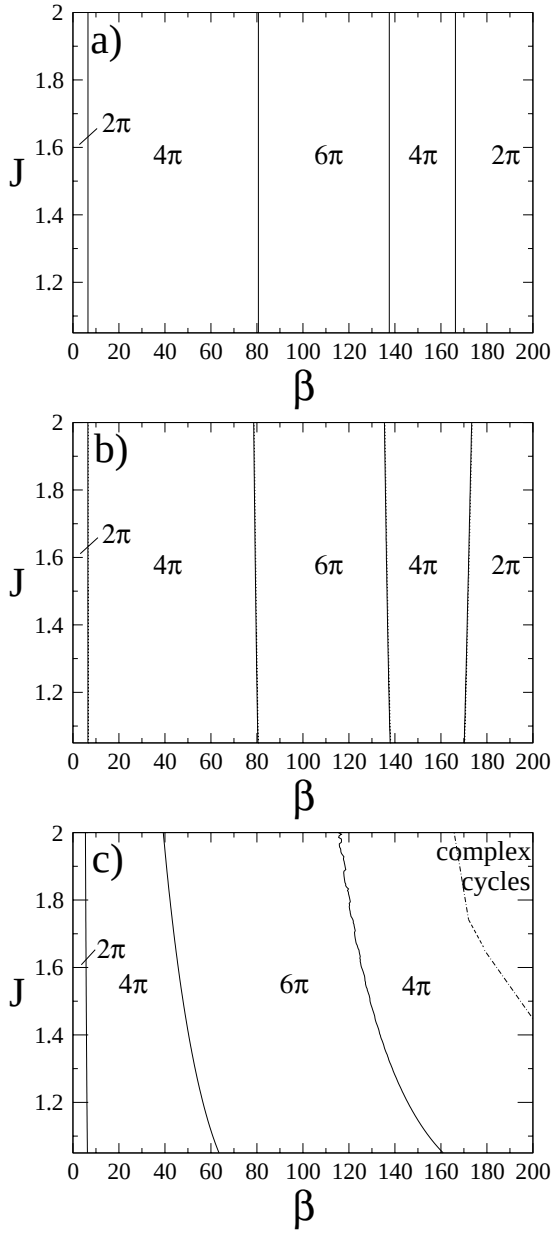

Fig. 11. Regions of phase jumps by multiples of 2π in the (β, J) parameter plane for a) $\gamma = 0$, b) $\gamma = 10^{-4}$, and c) $\gamma = 10^{-2}$.

motion. Since stable and unstable manifolds of saddles S_1 and S_2 are close to each other for large β (Figs. 10b–d), one can guess that the jump dynamics may depend sensitively on a nonzero small parameter γ . Moreover, for $\gamma > 0$ the regions of different jump length are expected to depend on J because J influences the slow variable u (see Eq. (10)). Yet, for $\gamma = 10^{-4}$, we still get a similar picture (Fig. 11b) in the (β, J) parameter plane although the lines separating different regions depend now on J as expected. The sensitivity of the dynamics with respect to the velocity of the slow motion (determined by γ) becomes more visible in Figure 11c for larger $\gamma = 10^{-2}$. A strong dependence of the shape and location of the borders

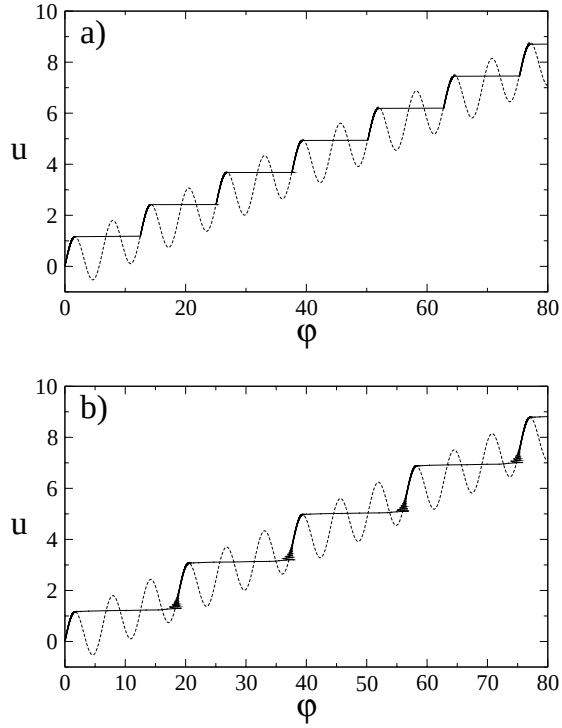

Fig. 12. Illustration of the sensitivity of the dynamics with respect to the velocity of the slow motion defined by parameter γ. For $\alpha = 10$, $\beta = 70$ and $J = 1.05$ one can find jumps a) by $\approx 4\pi$ at $\gamma = 10^{-4}$ and b) by $\approx 6\pi$ at $\gamma = 10^{-2}$. (The slow manifold is presented by a dashed line.)

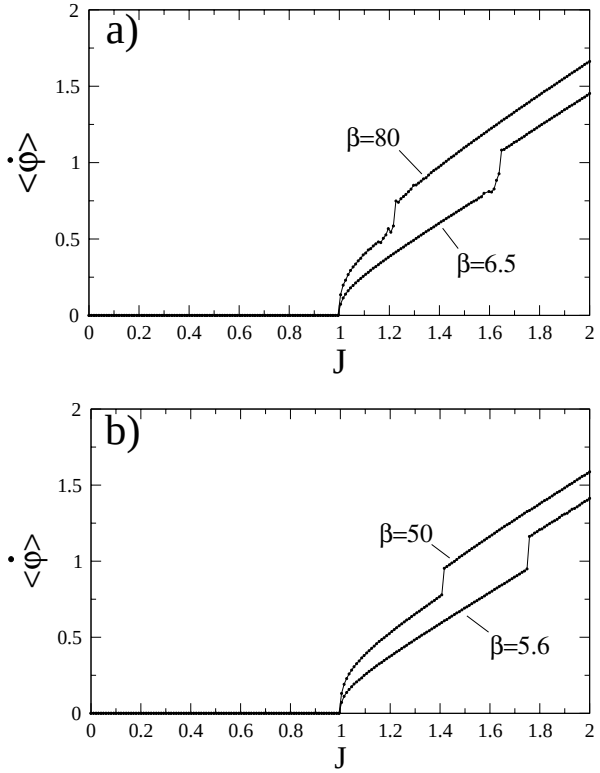

Fig. 13. The current-voltage characteristics for $\alpha = 10$ and a) $\gamma = 10^{-4}$, b) $\gamma = 10^{-2}$. At certain values of damping parameter β one observes sudden jumps in the mean voltage $\langle\dot{\varphi}\rangle$.

between different regions on J can be observed. Moreover, the region "complex cycles" in the right hand part of the plot contains such parameter points for which jumps of different lengths have been found to alternate.

We illustrate the different jump behavior in dependence on γ in Figure 12. For $\gamma = 10^{-4}$ we have found fast jumps by approximately 4π (Fig. 12a) whereas for $\gamma = 10^{-2}$ the jump length is about 6π (Fig. 12b). The other parameters are kept constant ($\beta = 70, J = 1.05$), and denote a parameter point that for $\gamma = 10^{-4}$ and $\gamma = 10^{-2}$ lies in different regions of phase jumps (see Figs. 11b, c). Thus, for $\gamma > 0$, one can hardly predict the transitions between different regions of phase jumps.

The current-voltage characteristics at intermediate values of damping parameter β show a feature caused just by sensitivity of the dynamics with respect to parameter γ. For certain values of β we observe sudden jumps in the current-voltage curves (see Figs. 13a, b). This is due to the J-dependence of jump regions of different length. If, by variation of J, one crosses a curve separating regions of different jump lengths in the (β, J) parameter plane (Figs. 11b, c), the jump length changes by approximately 2π and a sudden jump in the mean voltage occurs, correspondingly.

3.3 Low damping limit

In the low damping limit ($\beta \gg 1$) one can actually find the same features as for intermediate values of the damping parameter, like jumps of multiples of 2π, and also complex cycles. For $\beta \gtrsim 2000$ an additional feature in the current-voltage characteristics, namely hysteresis, can be observed [8]. In Figures 14a, b the current-voltage curves are presented for $\beta = 4000$ and $\beta = 5000$, respectively. For $\beta = 5000$ (Fig. 14b) the hysteresis is more pronounced than for the smaller value $\beta = 4000$ (Fig. 14a). Hysteresis can be observed if there exists bistability. Here, either the trajectory approaches a fixed point solution or a limit cycle in dependence on the initial condition.

Another feature, typical for large values of β, is the appearance of complex cycles. The reason is that the motion does not evolve on well separated time scales anymore. This can be explained as follows: If we only consider the jump dynamics without evolution of the slow variable u, then already for intermediate values of β, the oscillations rather slowly relax to the fixed point solution, as can be observed from Figures 10b–d. The time needed for the trajectory to become finally attracted to the fixed point increases with β. So, in the low damping limit, the relaxation time is non-negligible anymore and presents another time scale. It may happen that for large β these relaxation oscillations are not yet finished when the next fast jump in φ occurs. As a result, the time scales of slow and fast motion are not strictly separated anymore. This fact is a

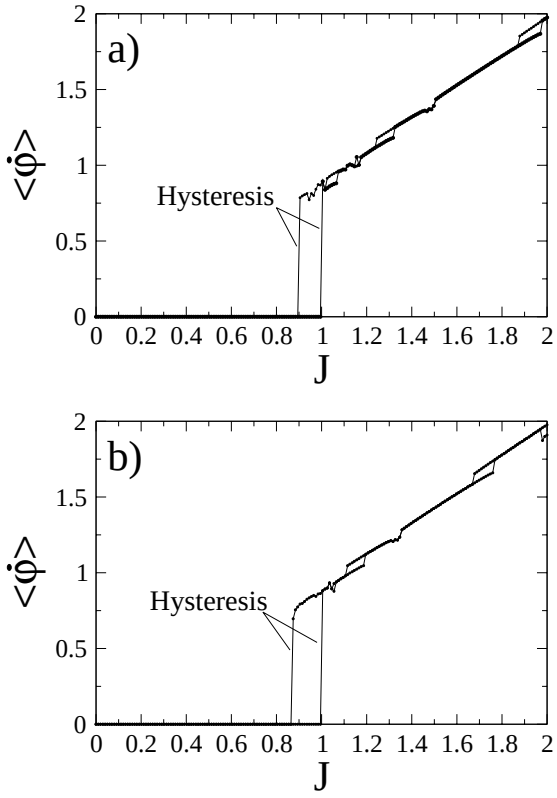

Fig. 14. The current-voltage characteristics in the low damping limit at $\alpha = 10$, $\gamma = 0.01$ and a) $\beta = 4000$ and b) $\beta = 5000$. The hysteresis is more pronounced for larger value of β.

reason for the appearance of complex cycles, and even of chaos in the autonomous Josephson junction. Figure 15a shows the current-voltage curve for $\beta = 2000$. Note that the hysteresis is not as much pronounced as for $\beta = 4000$ and $\beta = 5000$ (Fig. 14a, b). The maximum Lyapunov exponent has been computed in dependence on J in the same current interval, and its plot is presented in Figure 15b. In the current interval where the Josephson phase converges to a fixed point, the maximum Lyapunov exponent is less than zero. At $J = 1$ the dynamical behavior changes due to a bifurcation giving rise to a limit cycle characterized by zero maximum Lyapunov exponent. However, for certain values of J the maximum Lyapunov exponent becomes positive, thus chaotic behavior occurs there. Examples for nontrivial dynamical behavior are presented in Figure 16.

4 Conclusion

We have considered a Josephson junction model accounting a nonzero shunt inductance in series with the shunt resistance. This RCLSJ model is nearer to physical reality than the simpler RCSJ model. If the ratio of shunt resistance and intrinsic one serves as a small parameter, the Josephson junction model can be regarded as a nontrivial example for slow-fast dynamics. The strength of folding of the slow manifold depends on the inductance of the

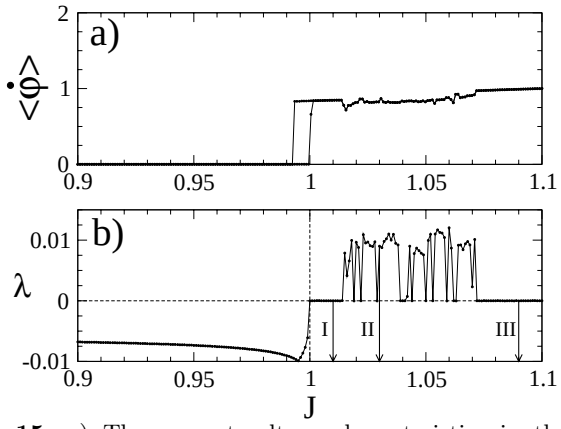

Fig. 15. a) The current-voltage characteristics in the low damping limit at $\alpha = 10$, $\gamma = 0.01$ and $\beta = 2000$. b) The maximum Lyapunov exponent in dependence on the net current J. The arrows mark the values of J for which the phase portraits are presented in Figure 16.

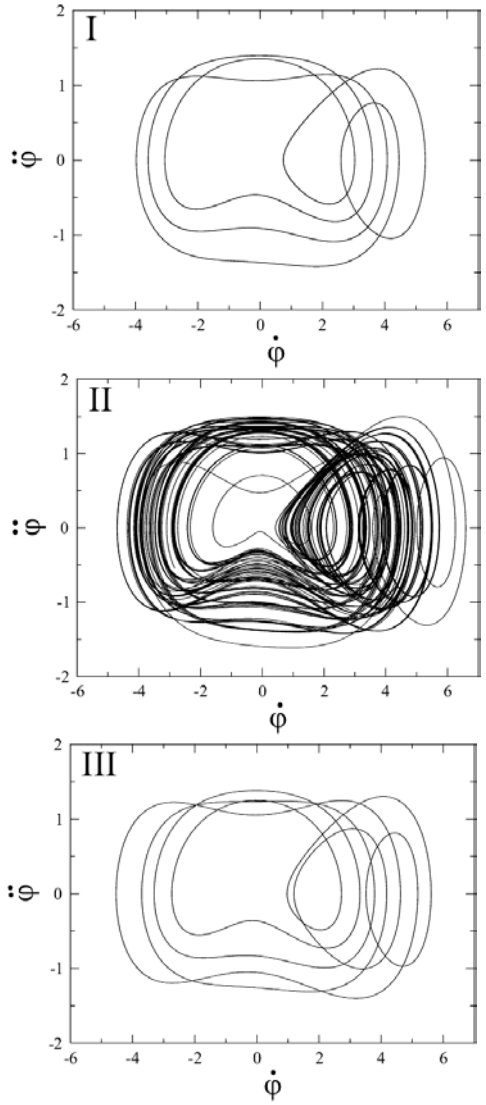

Fig. 16. Representative curves of nontrivial dynamical behavior for $\alpha = 10$, $\gamma = 0.01$ and $\beta = 2000$ and values of J sketched in Figure 15b. One finds at I) $J = 1.01$ a limit cycle, II) $J = 1.03$ chaotic behavior, and III) $J = 1.09$ a limit cycle.

shunt. If the shunt inductance is larger than the intrinsic one, then the slow manifold is folded and has many branches instead of the usual two as for instance in the van der Pol oscillator and the FitzHugh-Nagumo model. We have analysed the dynamics for high, intermediate and low damping, as well as the current-voltage characteristics for all three types of damping. For each type of damping the characteristics contains a supercurrent branch (for a net current smaller than a critical value) and a resistive one.

In the high damping limit, one obtains a system of two first-order differential equations with a small parameter. Here the fast motion is characterized by jumps in the Josephson phase by approximately 2π. For intermediate and low damping, even jumps by higher multiples can occur. Then, the fast motion is two-dimensional and there are different connections between saddles and foci. Due to the topology of these trajectories, which come closer to each other as the dissipation is lowered, the dynamics is sensitive to the velocity of the slow motion. The main manifestation of this sensitivity is the presence of vertical jumps in the current-voltage characteristics (Fig. 13).

For small dissipation, complex cycles have been observed, characterized by alternating jumps of different length. In the low damping limit, one can even observe chaos in the autonomous Josephson junction. The reason for the appearance of complex cycles and chaos is that a separation of time scales is not valid any more. Due to the possibility to transform the dimensionless parameters to corresponding values characterizing the Josephson junction, it is possible to check for the appearance of the reported phenomena in experiments.

We thank S. Kuznetsov, A. Shilnikov, and A. Ustinov for valuable discussions.

References

1. M. Kardar, Phys. Rev. B **33**, 3125 (1986)
2. J. Kim, W. G. Choe, S. Kim, H.J. Lee, Phys. Rev. B **49**, 459 (1994)
3. H. Eikmans, J.E. van Himbergen, Phys. Rev. B **41**, 8927 (1990)
4. K.K. Likharev, *Dynamics of Josephson Junctions and Circuits* (Gordon and Breach Publishers, NY, 1981)
5. C.B. Whan, C.J. Lobb, M.G. Forrester, J. Appl. Phys. **77**, 382 (1995)
6. C.B. Whan, C.J. Lobb, IEEE Trans. Appl. Supercond. **5**, 3094 (1995)
7. A.B. Cawthorne, C.B. Whan, C.J. Lobb, IEEE Trans. Appl. Supercond. **7**, 2355 (1997)
8. A.B. Cawthorne, C.B. Whan, C.J. Lobb, J. Appl. Phys. **84**, 1126 (1998)
9. S.K. Dana, D.C. Sengupta, K.D. Edoh, IEEE Trans. Circuits-I **48**, 990 (2001)
10. N.F. Rulkov, Phys. Rev. E **65**, 041922 (2002)
11. D.E. Postnov, O.V. Sosnovtseva, S.Y. Malova, E. Mosekilde, Phys. Rev. E **67**, 016215 (2003)